Check for updates

ADVANCED ENERGY MATERIALS
www.advenergymat.de

All-Fabric Direct-Current Triboelectric Nanogenerators Based on the Tribovoltaic Effect as Power Textiles

Tianmei Lv, Renwei Cheng, Chuanhui Wei, Erming Su, Tao Jiang, Feifan Sheng, Xiao Peng, Kai Dong, and Zhong Lin Wang**

The tribovoltaic effect is the direct-current (DC) output that results from sliding a p-type semiconductor on top of an n-type semiconductor, and it is caused by the electron–hole pairs generated However, the rigid structure of traditional semiconductor limits its potential application in wearable fields. Here, p–type and n–type fabric with semiconductor properties are prepared by doping small organic molecules of cetyltrimethylammonium bromide and sodium dodecylbenzene sulfonate on the carbon atoms of single–wall carbon nanotubes (SWCNTs), and three all-fabric direct-current triboelectric nanogenerators based on the tribovoltaic effect (AFDC-TENG) are developed , which exhibit high flexibility, satisfactory comfort, and stable DC output. In addition, the effects of structural parameters and environmental factors on the electrical output of AFDC-TENG are systematically discussed. The output voltage, current, and power density of p-type AFDC-TENG can reach 0.2 V, 0.29 µA, and 45.5 mV m^{-2} at a maximum speed of 0.2 m s^{-1} and a sliding frequency of 1 Hz, respectively. This work proposes a simple and scalable design form for all-fabric DC power supply devices, which has potential applications in the future micro/nano energy or self-powered flexible sensors.

1. Introduction

Decentralized electronics that have emerged with the Internet of Things, exacerbate the contradiction between distributed energy needs and traditional centralized energy supply. Widely used batteries need to be replaced frequently and are not friendly to environment, which is difficult to meet the future demand of sustainable and environmentally friendly energy.[1] Moreover, the decreasing power consumption also gives opportunities for some wearable energy harvesters, such as solar cells, thermoelectric generators, electromagnetic generators, piezoelectric nanogenerators, and triboelectric nanogenerators (TENGs).[2] Solar cells and thermoelectric generators are greatly limited by the environment. The magnetic metal particles in electromagnetic generators will increase the weight of wearable devices, which is unfavorable for wearing comfort. Piezoelectric nanogenerators show low power output due to low charge density. As an emerging energy harvesting method, TENG can convert the human biomechanical energy into electrical energy based on the coupling effects of triboelectrification and electrostatic induction, which has the advantages of environmental friendliness, low cost, and wide selection of materials.[3]

However, the charge in traditional TENGs based on electrostatic induction does usually give an alternating current (AC) output.[4] Recently, several methods have been developed to achieve DC output TENGs, including rectifier bridges,[5] mechanical switches,[6] tribovoltaic effect,[7] and air breakdown effect.[8] Rectifier bridges are currently the most widely used due to their convenience. However, the power consumption of the rectifier bridge cannot be ignored, and the hard rectifier bridge is not friendly to wearable applications. The DC signal of the mechanical switching strategy generally relies on the alternating connection of the two electrodes of the TENG and the two electrodes of the external circuit, which presents a great challenge to the structural design of flexible fabrics.[9] DC-TENG based on the air breakdown effect requires high surface charge densities under large loads, which will greatly affect the durability of friction materials. Moreover, it is difficult to avoid the high internal resistance of TENGs through the above methods.

T. Lv, E. Su
School of Chemistry and Chemical Engineering
Guangxi University
Nanning 530004, P. R. China

T. Lv, R. Cheng, C. Wei, E. Su, T. Jiang, F. Sheng, X. Peng, K. Dong, Z. L. Wang
CAS Center for Excellence in Nanoscience
Beijing Key Laboratory of Micro-Nano Energy and Sensor
Beijing Institute of Nanoenergy and Nanosystems
Chinese Academy of Sciences
Beijing 101400, P. R. China
E-mail: dongkai@binn.cas.cn; zhong.wang@mse.gatech.edu

R. Cheng, C. Wei, T. Jiang, F. Sheng, X. Peng, K. Dong
School of Nanoscience and Engineering
University of Chinese Academy of Sciences
Beijing 100049, P. R. China

Z. L. Wang
School of Material Science and Engineering
Georgia Institute of Technology
Atlanta, GA 30332-0245, USA

The ORCID identification number(s) for the author(s) of this article can be found under https://doi.org/10.1002/aenm.202301178

DOI: 10.1002/aenm.202301178

 © 2023 Wiley-VCH GmbH

The tribovoltaic effect is based on the directional movement of electron–hole pairs under the built-in electric field at the interface between semiconductors/metals/liquids and semiconductors.[10] DC-TENGs based on the tribovoltaic effect typically require two contact or friction materials, resulting in simple structural design and overall fabrication. Furthermore, the intrinsic impedance of DC-TENGs based on the tribovoltaic effect is usually ≈10 MΩ, much less than that of the alternating current TENGs.[11]

It can be found that DC-TENGs based on tribovoltaic effect include at least one semiconductor. Currently, most of the research focus on silicon-based semiconductors due to their stable semiconductor performance and mature industrialization.[10b,12] However, silicon-based semiconductors exhibit rigid and brittle structural characteristics on a macro scale, which limits the wearable applications in silicon-based DC-TENGs.[13] Therefore, researchers are gradually turning to flexible semiconductors to design flexible DC-TENGs based on tribovoltaic effect.[14] For example, Meng et al. reported a flexible DC-TENG based on a dynamic schottky junction between an aluminum slider and a poly(3,4-ethylene dioxythiophene) (PEDOT)-coated fabric.[15] However, the application of inherent brittle and rigid metal films in this work restrict its stability and comfort as a wearable product. Organic polymers such as PEDOT and polypyrrole (PPy) are commonly used as p-type semiconductors to prepare flexible nanogenerators to provide DC output.[14c,16] Although great success has been achieved in obtaining p-doped organic semiconductors, the development of effective n-doped organic semiconductors is still slow due to the lack of stable and processable n-type dopants. Carbon nanotubes (CNTs) possess both metal conductivity and semiconductor properties, which are mainly related to their diameter and spiral structure. Compared with sp^3 hybridization, carbon atoms of CNTs adopt sp^2 hybridization, which exhibit a relatively substantial s-orbital component.[17] Furthermore, CNTs possess a high specific surface area and exhibit strong adsorption properties, enabling them to adsorb electron acceptor or donor dopants, such as organic small molecules or polymers, onto the sp^2 structure. Therefore, it is very likely that SWCNTs can be doped with organic molecules to obtain p- or n-type semiconductor effects.[18] In addition, small molecular doping approaches can simultaneously improve the charge transporting and electrical properties of organic semiconductors. It was found that poly(ethyleneimine), poly(vinylpyrrolidone), and a series of amines with crown ethers, such as mino-substituted rylene dimides and diethylenetriamine, are suitable as n-type dopants for CNTs.[19] However, most of these doping treatments are expensive, complex, difficult to process, or insoluble in water. Due to the natural wearability and indispensability of fabrics, the convenient and low-cost method of developing AFDC-TENG may be an ideal solution of wearable energy harvesters compared to that with the existence of hard silicon-based materials and metal films.[10a,20]

Here, three kinds of flexible and breathable AFDC-TENGs are designed based on the tribovoltaic effect of semiconducting materials, which can directly convert mechanical energy into DC electrical output. We propose a simple solution-processing method to achieve p- or n-type organic semiconductors by doping SWCNTs with organic small molecules. The conventional cotton fabric substrates are immersed in p- and n-type SWCNTs to obtain p- and n-type fabrics, respectively. Each of the three kinds of functional fabrics (Ni-coated conductive fabric, p-type, and n-type semiconductor fabric) can generate DC output by reciprocating friction mode, which provides us with greater freedom in selecting device combinations. During sliding contact, a dynamic Schottky contact is formed between the Ni-coated conductive fabric and the p- or n-type SWCNTs-coated fabric. A large number of non-equilibrium electron–hole pairs at the two interfaces are excited after absorbing the energy released by the friction of atom–atom bonds, and they are separated by the built-in electric field. Then, the carriers are driven by the built-in electric field to move in a directional manner and form a unidirectional current. In this work, the friction between p-type fabric and conductive fabric can output a voltage of 0.2 V, a current of 0.29 μA, and an output power density of 45.5 mW m^{-2} at a maximum speed of 0.2 m s^{-1} and a sliding frequency of 1 Hz. In addition, its output current increases linearly when increasing the applied pressure and sliding speed. Moreover, AFDC-TENGs also demonstrate excellent flexibility, breathability, and durability. This work provides a broad application prospect for the future application of wearable power sources.

2. Results and Discussion

In this work, two functional fabrics with p- and n-type semiconductor attributes are prepared by depositing SWCNTs doped with different types of organic small molecules on the fabric substrates. As shown in **Figure** 1a, three kinds of AFDC-TENGs based on the tribovoltaic effect of semiconductor materials are developed by rubbing the n-type fabric with a Ni-coated conductive fabric (defined as N/Ni–F), the p-type fabric with a Ni-coated conductive fabric (defined as P/Ni–F), or the p-type fabric with the n-type fabric (defined as p/n), respectively. More details can be found in Figure S1 (Supporting Information). Each of the three kinds of functional fabrics can generate DC output by reciprocating friction mode. Furthermore, the AFDC-TENG can be directly integrated on our garments to harvest biomechanical energy, drive low-power wearable electronics, or detect human physiological signals. Pristine SWCNTs exhibit p-type characteristic due to the oxygen impurity in the atmosphere.[21] By judicious doping with certain organic small molecules or polymers with electron acceptors or donors, SWCNTs can be rationally designed as either p- or n-type doped, which can increase the concentration of charge carriers in semiconductors through the transfer of electrons from dopants to organic small molecules (the major carriers are positively or negatively charged). This is due to the extra free carriers (holes or electrons) generated in their corresponding valence or conduction bands. As shown in Figure 1b, p- and n-type conversion is achieved by doping organic small molecules SDBS and CTAB on SWCNTs, respectively. Compared with the traditional doping arsenic atom and boron atoms in pure silicon base, the method of using organic small molecules doped SWCNTs exhibits simpler operation and broader scalability. In detail, by adding cetyltrimethylammonium bromide (CTAB) and sodium dodecylbenzene sulfonate (SDBS) to the pure SWCNTs water dispersed solution, a large number of Br anions and Na cations are introduced around SWCNTs, respectively, to achieve n- and p-type SWCNTs (Figure S2, Supporting Information). Due to the opposite of the particle

© 2023 Wiley-VCH GmbH

16146840, 0, Downloaded from https://onlinelibrary.wiley.com/doi/10.1002/aenm.202301178 by Georgia Institute Of Technology, Wiley Online Library on [15/06/2023]. See the Terms and Conditions (https://onlinelibrary.wiley.com/terms-and-conditions) on Wiley Online Library for rules of use; OA articles are governed by the applicable Creative Commons License

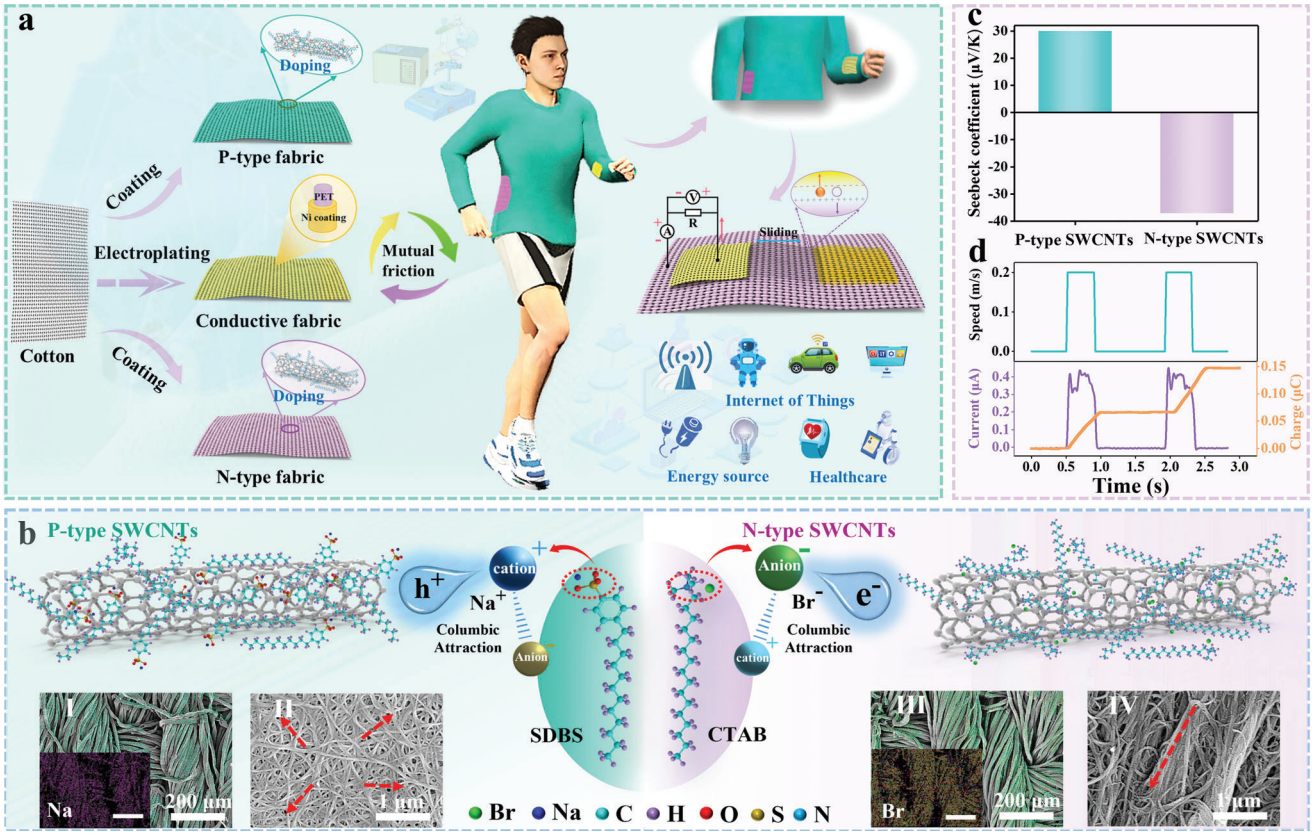

Figure 1. Preparation process, application scenarios, and structures of the AFDC-TENG. a) Preparation process, application scenarios and compositions of energy harvesting clothes. b) Chemical structures of studied dopants and p- and n-type materials for p- and n-doping in this study. In Figure b-I,III) represents SEM images of the p- and n-type fabric with EDX elemental mappings, respectively. II,IV) represents SEM images of the p- and n-type SWCNTs, respectively. c) Seebeck coefficients of n- and p-type SWCNTs. d) Speed and current of the N/Ni–F as a function of time.

electrical properties produced by the two doping agents in the aqueous solution, the doped SWCNTs show different semiconductor properties and surface appearances. The effect of dispersion medium on the doped SWCNT morphology was compared. The well-dispersed P-doped and N-doped SWCNTs exhibit similar tightly packed network structures, which effectively facilitate carrier transport. The SWCNTs on the surface of p-type fabric displays uniform distribution (Figure 1b-II). In the n-type SWCNTs, the state of the CTAB dispersion and the coating behavior for the CTAB-doped SWCNTs is shown (Figure 1b-IV), indicating that sufficient CTAB micelles are formed on the SWCNTs surface, due to the anion-induced electron transfer between the bromide anions (Br^-) of CTAB on SWCNTs. we found that CTAB could change the majority of charge carriers of SWCNTs from holes to electrons, resulting in the formation of n-type SWCNTs. Both the p- and n-type SWCNTs achieve effective dispersion and uniform distribution of the surface of cotton fabric. However, unlike the random orientation of the p-type SWCNTs, the n-type SWCNTs exhibit a regular orientation. As shown in Figure S3 (Supporting Information) and Figure1b-I,III, SEM images and corresponding energy-dispersive X-ray spectrometry (EDX) indicate the existence of uniform elemental distribution. In addition, the two organic small molecules and SWCNTs have been confirmed to bind uniformly to the surface and interior of the cotton fabric. When using CTAB as the cationic dopant, it adsorbs and covers the surface of SWCNTs, which hinders the collision of oxygen molecules with SWCNTs.

The Seebeck coefficient can be used to characterize the magnitude of the Seebeck effect. The expression is:

$$S = dV/Dt \tag{1}$$

where dT is the temperature difference between two points on the thermoelectric material. dV is the thermo-electromotive force between the corresponding two points. In thermoelectric materials, when electrons are multi-carrier, the cold end is negative, and S is negative. On the contrary, when the hole is multi-carrier, S is a positive value. As illustrated in Figure 1c, n-type SWCNTs exhibits a negative Seebeck coefficient due to higher electron transfer rate between bromide ions in CTAB and SWCNTs than that between SWCNTs and oxygen molecules, resulting in the formation of multiple electrons in SWCNTs. which is different from pure SWCNTs and p-type SWCNTs. In order to further clarify the mechanism of n-type doping, we conducted Raman spectroscopic analysis of p- and n-type SWCNTs (Figure S4, Supporting Information). Compared to the G band at 1593 cm^{-1} in the Raman spectrum of p-type SWCNTs, the D band at 1342 cm^{-1} exhibits a lower intensity. Compared to p-type SWCNTs, the n-type SWCNTs exhibit similar relative intensities with a very week D band at 1340 cm^{-1} and a stronger G band at 1588 cm^{-1}. This

© 2023 Wiley-VCH GmbH

16146840, 0, Downloaded from https://onlinelibrary.wiley.com/doi/10.1002/aenm.202301178 by Georgia Institute Of Technology, Wiley Online Library on [15/06/2023]. See the Terms and Conditions (https://onlinelibrary.wiley.com/terms-and-conditions) on Wiley Online Library for rules of use; OA articles are governed by the applicable Creative Commons License

confirms that there are almost no structural defects during the doping process. Furthermore, the RBM regions of n- and p-type SWCNTs exhibit nearly equal intensity, indicating that there is no notable hindrance to the radial oscillation of carbon atoms. As discussed above, CTAB is a highly effective negative dopant for SWCNTs. In order to manufacture optimal p- and n-type SWCNTs, various mass ratios of SWCNT: surfactant were added to DI water as the dispersion medium. Figure S5 (Supporting Information) shows the current output during the sliding process of p– or n-type fabrics and Ni-coated conductive fabric at different mass ratios. It can be seen from the diagram that a very low amount of SDBS and CTAB does not contribute to good dispersion of SWCNTs and leads to low-quality current output. As is observed, the 10: 10 mg mg^{-1} mass ratio showed the highest current output for p- and n-type fabrics, respectively. When the mass ratio of SWCNTs: surfactants gradually increase, a decrease in electrical output is observed as more dielectric SDBS and CTAB molecules interfere among the conductive SWCNTs (SDBS and CTAB are electrically insulating). The effects of different dip-coating times on the output of p- and n-type AFDC-TENG are compared (Figure S6, Supporting Information). For p-type AFDC-TENG, fewer SWCNTs particles are deposited on cotton fabrics when the soaking time is 20 s, and the coverage of SWCNTs on cotton fabrics will reduce, reducing the electrical output. However, with the increase of dipping time. The SWCNTs deposited on the cotton fabric reach saturation and the output reaches stability when it reaches 60 s. Therefore, the best dipping time is 60 s. For n-type AFDC-TENG, a similar phenomenon can be observed, and the optimal dip-coating time is also 60 s. In addition, the open-circuit voltage (V_{OC}), short-circuit current (I_{SC}), and short-circuit charge transfer (Q_{SC}) of SWCNTs-coated fabrics without organic small molecules were discussed (Figure S7, Supporting Information). Compared with the fabrics doped with SDBS and CTAB, the undoped SWCNTs coated fabric possesses p-type characteristics due to oxygen impurities in the atmosphere. the I_{SC}, V_{OC}, and Q_{SC} are 0.1 μA, 0.12 V, and 0.035 μC, respectively. Its electrical output is greatly reduced. Undoped fabrics have relatively few electrons and holes. Therefore, the introduction of small organic molecules on the surface of SWCNTs can effectively improve output performance. We have demonstrated that the n-type fabric and Ni-coated conductive fabrics are used as a couple of triboelectric layers, and DC electricity outputs caused by the tribovoltaic effect. Figure 1d depicts the changes in speed and output current, charge versus time during a complete cycle. At a sliding speed of 0.02 m s^{-1}, Peak current and peak charge are ≈0.28 V and 0.15 μC, respectively. The AFDC-TENG exhibits a relatively continuous and stable DC signal output throughout the whole motion cycle. In addition, Figure S8 (Supporting Information) also shows the variation of speed and output voltage with time. The mechanical properties of the AFDC-TENG are also evaluated. As demonstrated in Figure S9 (Supporting Information), various kinds of complex mechanical deformations, such as folding and twisting are conducted, which demonstrates its excellent flexibility. For wearable textile electronics, air breathability is the basis for human wearable comfort. Under a pressure difference of 50 Pa and an area of 5 cm^2, the air breathability of n- and p-type fabrics is as high as 663.8 and 669.2 mm s^{-1}, respectively (Figure S10, Supporting Information). Compared with commercial cotton fabrics (air breathability: 707.4 mm s^{-1}), it was found that the breathability of n- and p-type fabrics is very high, sufficient to meet the comfort needs of daily wear.

To examine the impact of various frequencies on the output of AFDC-TENG, p- and n-type SWCNTs were dipped onto cotton fabric to compare and analyze the output performance of P/Ni–F, N/Ni–F, and P/N under friction in this study. The 3D schematic diagram of triboelectric charges generated by P/Ni–F sliding is shown in **Figure 2**a. The direction of the external circuit current flows from the p-type fabric to the Ni-coated conductive fabric. In addition, a schematic diagram of the tribo-current generation caused by the tribovoltaic effect is also given. When the Ni-coated conductive fabric collides with the atoms belonging to the p-type fabric surface, the energy is released due to the formation of bonds at the interface, named as "bindington". Then the electrons–hole pair will be excited by "bindington" and separated by the built-in electric field at the Ni-coated conductive fabric and the p-type fabric interface. Electrons and holes are transferred to the Ni-coated conductive fabric side and p-type fabric type side, respectively. This can accumulate to induce potential differences at the interface, resulting in voltage and current output through the external circuit. In addition, the 3D schematics of N/Ni–F and P/N and the schematic diagram of the generation of tribo-current are supplemented (Figure S11, Supporting Information). For N/Ni–F, the direction of the external circuit current flows from the Ni-coated conductive fabric to the n-type fabric. Electrons and holes are transferred to the Ni-coated conductive fabric side and the n-type fabric side, respectively. For P/N, the current direction flows from n-type fabric to p-type fabric through the external circuit. The electron–hole pair is separated by the interface between the n-type fabric and the p-type fabric under the action of the built-in electric field. Thus, electrons and holes are transferred to the n-type fabric side and the p-type fabric side, respectively. For P/Ni–F, N/Ni–F, and P/N, depletion regions are formed at the contact interface due to differences in Fermi energy levels. And the electrical properties of the depletion region have certain rectification characteristics. As shown in Figure 2b, the *I–V* curves of the P/Ni–F, N/Ni–F, and P/N are tested to determine the depletion regions at the two interfaces. The results show that the *I–V* curves of the P/Ni–F, N/Ni–F, and P/N are asymmetric and nonlinear, indicating the formation of depletion regions at the interfaces of P/Ni–F, N/Ni–F, and P/N. This is due to the existence of the Schottky barrier, which forms unidirectional electronic conductivity in the interface. In the DC-TENGs, when the Schottky contact interface is in equilibrium, the electrons and currents emitted by the metal and semiconductor on both sides of the interface are equal in magnitude but in opposite direction. This balance creates a dynamic equilibrium in which no current flows. When subjected to a positive bias voltage, electrons and holes migrate toward the Schottky junction and recombine, resulting in a current corresponding to their movement. The current increases with the increasing of the applied voltage. The current density (*J*) at the Schottky contact interface under positive bias voltage can be mathematically expressed as follows:

$$JS = A^* T^2 \exp\left(-\frac{q\varphi}{k_0 T}\right)\left[\exp\left(\frac{qV}{k_0 T}\right) - 1\right] \quad (2)$$

© 2023 Wiley-VCH GmbH

16146840, 0, Downloaded from https://onlinelibrary.wiley.com/doi/10.1002/aenm.202301178 by Georgia Institute Of Technology, Wiley Online Library on [15/06/2023]. See the Terms and Conditions (https://onlinelibrary.wiley.com/terms-and-conditions) on Wiley Online Library for rules of use; OA articles are governed by the applicable Creative Commons License

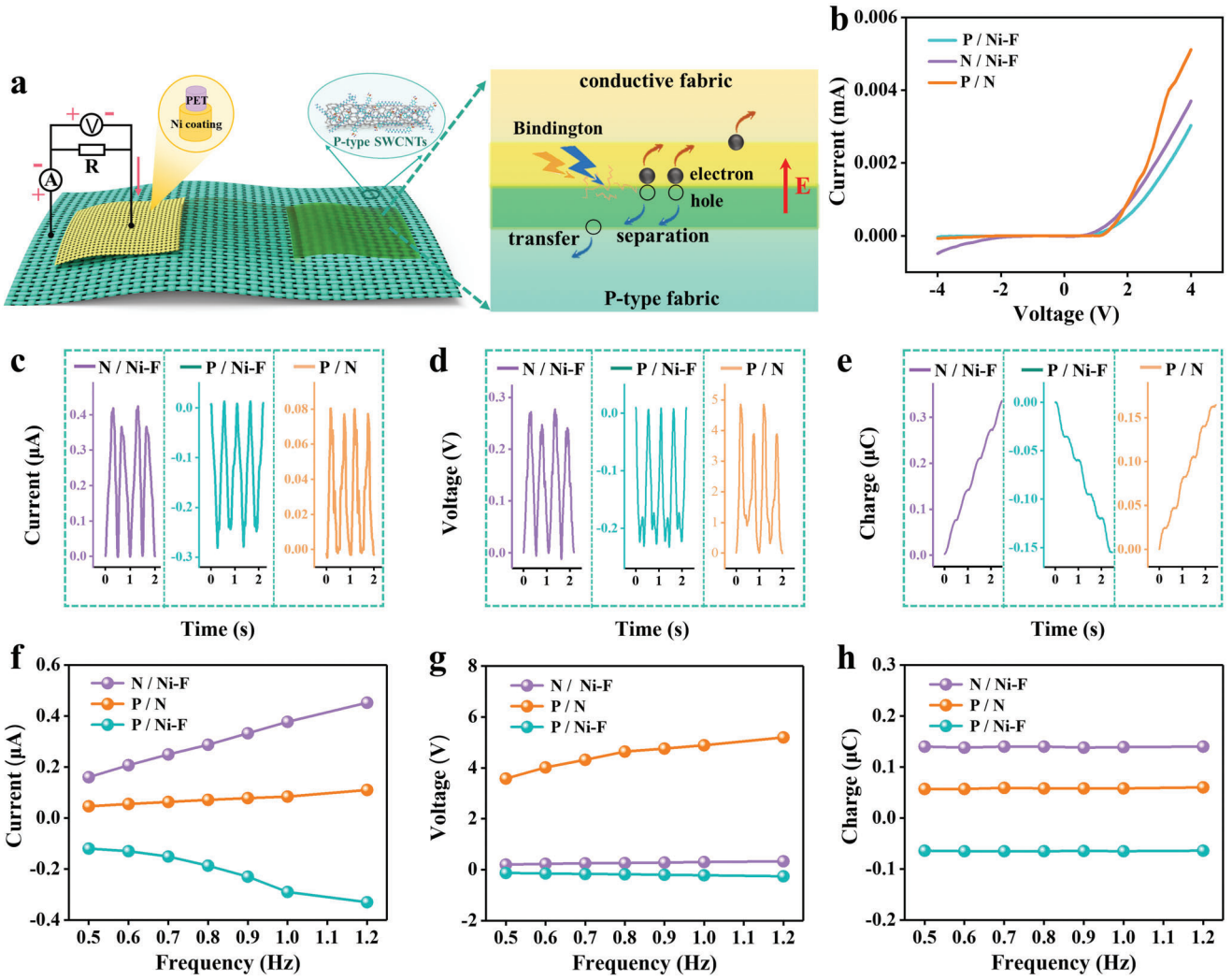

Figure 2. Influence of three types of AFDC-TENG on electrical output at different frequencies. a) 3D schematic diagram of the p-type AFDC-TENG and a schematic diagram of the generation of tribo-current. b) *I–V* curve of the P/Ni–F, N/Ni–F, and P/N. c–e) V_{OC}, I_{SC}, and Q_{SC} outputs of P/Ni–F, N/Ni–F, and P/N. f–h) The output of V_{OC}, I_{SC}, and Q_{SC} at different frequencies.

$$A^* = \frac{4\pi q m_n^2 k_B^2}{h^2} \tag{3}$$

where A^* represents the effective Richardson constant, T is the temperature, q is the elementary charge, V is the applied voltage, k_0 is the Boltzmann constant, qV is the potential barrier height variation caused by the surface electric field E, and $q\varphi$ is the height of the potential barrier.

A measuring platform is established to study the electrical output performance of the three types of AFDC-TENGs. When measuring P/Ni–F and N/Ni–F, p-type or n-type fabric with the size of 150 cm^2 is fixed on an acrylic board. A Ni-coated conductive fabric is attached to another acrylic board, which is fixed to the vibrating surface of a linear motor. The same is true when measuring P/N. When the linear motor operates back and forth, P/Ni–F, N/Ni–F, and P/N are periodically rubbed. The V_{OC}, I_{SC}, and Q_{SC} of the three AFDC-TENGs are measured. It can be found that the opposite V_{OC}, I_{SC}, and Q_{SC} are generated when P/Ni–F and N/Ni–F rub. As shown in Figure 2c–e, at a sliding frequency of 1 Hz, the I_{SC} of P/Ni–F, N/Ni–F, and P/N can reach 0. 29 μA, 0.42 μA, and 80 nA respectively, V_{OC} can reach 0.24, 0.28, and 4.8 V respectively, and Q_{SC} is ≈0.07, 0.15, and 0.05 μC, respectively. The work function changes, due to SWCNTs are doped with organic small molecule, which directly affects the magnitude and direction of electrical output. In this work, the work function of SWCNTs semiconductor was calculated through the measurement of ultraviolet photoelectron spectroscopy (UPS) (Figure S12, Supporting Information). The calculation formula is:

$$W = h\nu - E_{cutoff} \tag{4}$$

where W represents the work function, $h\nu$ is excitation source energy (it is a constant of 21.2 eV), E_{cutoff} is secondary electron emission cut-off edge. It is shown that the n-type fabric has a lower work function (W_N: 4.53 eV) than Ni-coated conductive fabrics (W_{Ni-F}: 4.6 eV), while the p-type fabric has a higher work

© 2023 Wiley-VCH GmbH

16146840, 0, Downloaded from https://onlinelibrary.wiley.com/doi/10.1002/aenm.202301178 by Georgia Institute Of Technology, Wiley Online Library on [15/06/2023]. See the Terms and Conditions (https://onlinelibrary.wiley.com/terms-and-conditions) on Wiley Online Library for rules of use; OA articles are governed by the applicable Creative Commons License

function (W_p: 4.63 eV) than Ni-coated conductive fabrics. When the N/Ni–F rubs, the positive charge is located on the n-type fabric, the current will flow from the Ni-coated conductive fabric to n-type fabric in the external circuit under the electrostatic field. When the P/Ni–F rubs, the positive charge is located on the Ni-coated conductive fabric and the current will flow from p-type fabric to Ni-coated conductive fabric. This explains why opposite V_{OC}, I_{SC}, and Q_{SC} output when p- and n-type fabrics and Ni-coated conductive fabric rub. In addition, P/N has a higher output voltage and low current than P/Ni–F and N/Ni–F. This discrepancy may be due to the influence of surface static electricity, which may result in the formation of interface electric fields.[22] The results demonstrate that an increase in frequency will lead to an increase in current and voltage, while the charge remains nearly constant (Figure 2f). The reason can be attributed to the fact that as the sliding frequency increases, more triboelectric charges are released at the Schottky interface, which excites more electrons and holes. The slight increase in voltage may be due to the increase in contact area during the sliding process, resulting in an increase in electron hole pairs (Figure 2g). This shows that the increase of sliding frequency has an impact on the output. The reason why the charge remains almost unchanged is that the sliding area remains unchanged during the sliding process (Figure 2h). Compared with AC-TENG, textile DC generators make it easier to integrate into our clothes to collect human mechanical energy. Three kinds of AFDC-TENG based on the tribovoltaic effect of semiconductor materials were prepared. All three functional fabrics can generate DC output by reciprocating friction, and their output performance is also shown in Table S1 (Supporting Information).

Figure 3 depicts the working mechanisms of the three types of AFDC-TENGs. Due to the different work functions of the three fabrics, built-in electric fields will be formed at the interface of P/Ni–F, N/Ni–F, and P/N on the time of contact, resulting in a redistribution of interface carriers. In this work, the working principles of DC power generation during the sliding process of the three AFDC-TENGs are investigated and analyzed in detail. For the N/Ni–F contact mode, the work functions of n-type fabric and Ni-coated conductive fabric are discrepant ($W_{Ni–F} > W_N$), which leads to difference in Fermi energy level. At the moment when the interface of N/Ni–F is formed, the Fermi level of n-type fabric will decrease, while that of conductive fabric will rise, which will promote the flow of electrons from the n-type fabric to the Ni-coated conductive fabric. Finally, the Fermi levels of both n-type fabric and conductive fabric will reach equilibrium, and the electrons will not flow relatively. During this process, a build-in electric field will be generated in the interface between the N/Ni–F, and the direction of which is from the n-type fabric to conductive fabric. In addition, in the final state of thermodynamic equilibrium, the number of electrons and holes generated is equal to the number of recombination losses. In this case, there is no obvious flow of carriers in the semiconductor and no external current is detected (Figure 3a). When the two fabrics slide relatively, the destruction and reconstruction of atomic bonding will occur continuously at the interface. The energy dissipation during atomic bonding causes the generation of new electron–hole pairs. The electrons are excited to transition to the conduction band, and the equivalent holes are located in the valence band, which indicates that the thermodynamic equilibrium state is broken (Figure 3b). The newly generated electron–hole pairs separate under the action of the built-in electric field. The electrons flow to conductive fabric, while the holes flow to the n-type fabric, and the current from the Ni-coated conductive fabric to the n-type fabric is formed in the external circuit. To further elucidate the electronic transfer process of N/Ni–F, we adopt the concept of electron cloud-potential well. As shown in Figure S13 (Supporting Information), before the N/Ni–F contacts, the electron cloud remains separated and do not overlap. When N/Ni–F contacts and rubs against each other, their electron clouds gradually interact and overlap. Under the action of strong electron clouds overlapping, the intermediate energy potential barrier is reduced, and then the electrons jump from the Ni-coated conductive fabric to the n-type fabric. Therefore, the charge transfer is achieved.[23] Similarly, the same applies to P/Ni–F and P/N.

The working mechanism of P/Ni–F is similar to that of N/Ni–F. Since the work function of Ni-coated conductive fabric is less than that of p-type fabric ($W_{Ni–F} < W_p$), during the contact process, the Ni-coated conductive fabric releases electrons and the p-type fabric receive electrons until the electrons in N/Ni–F are in equilibrium. In addition, due to the difference in Fermi energy levels between the two fabrics, the energy band of p-type fabric will bend upward after contact, and the direction of the internal electric field is from the Ni-coated conductive fabric to p-type fabric, as shown in Figure 3c. When P/Ni–F slides, a Schottky barrier is formed in the depletion zone of the p-type fabric. The sliding kinetic energy releases a large number of non-equilibrium carriers, which stimulate electron and hole pairs under the action of the internal electric field and form a current through the external circuit. The direction of the current flows from p-type fabric to Ni-coated conductive fabric (Figure 3d). These principles explain why N/Ni–F and P/Ni–F have opposite currents. Second, the principle of P/N contact are also investigated. Due to the fact that the Fermi level of n-type fabrics is higher than that of p-type fabrics, when P/N contacts to form a P–N junction, electrons flow from the N-region of the high Fermi level to the P-region of the low Fermi level, leading to that the Fermi level of n-type fabric (E_{FN}) moves down and the Fermi level of p-type fabric (E_{FP}) moves up to form a unified Fermi level, and the conduction band and valence band of the P-region and N-region become curved (Figure 3e). When a p-type fabric slides over an n-type fabric, p-type fabric lose electrons and n-type fabric gain electrons. Static charges will appear at the interface between them, with positive charges located on the p-type fabric. Under the action of electrostatic field, electric current will flow from n-type fabric to p-type fabric in the external circuit (Figure 3f).

To fully understand the AFDC-TENG, the p-type AFDC-TENG was elected to systematically investigate the influence of various parameters, including friction layer material, contact area, applied pressure, and long-term stability. Therefore, we measure the electrical output by varying the above experimental parameters. Considering the triboelectric layer is the source of the electrical output of the p-type AFDC-TENG. The influence of different substrates is explored, including polyester, polyester–cotton, and cotton. The coating time and area are kept constant. It is found that selecting cotton fabric as the substrates can lead to a higher electrical output compared to polyester and polyester–cotton (**Figure 4**a). This may be due to the strong moisture-absorbing ability of cotton fabrics when preparing p- and n-type

© 2023 Wiley-VCH GmbH

16146840, 0, Downloaded from https://onlinelibrary.wiley.com/doi/10.1002/aenm.202301178 by Georgia Institute Of Technology, Wiley Online Library on [15/06/2023]. See the Terms and Conditions (https://onlinelibrary.wiley.com/terms-and-conditions) on Wiley Online Library for rules of use; OA articles are governed by the applicable Creative Commons License

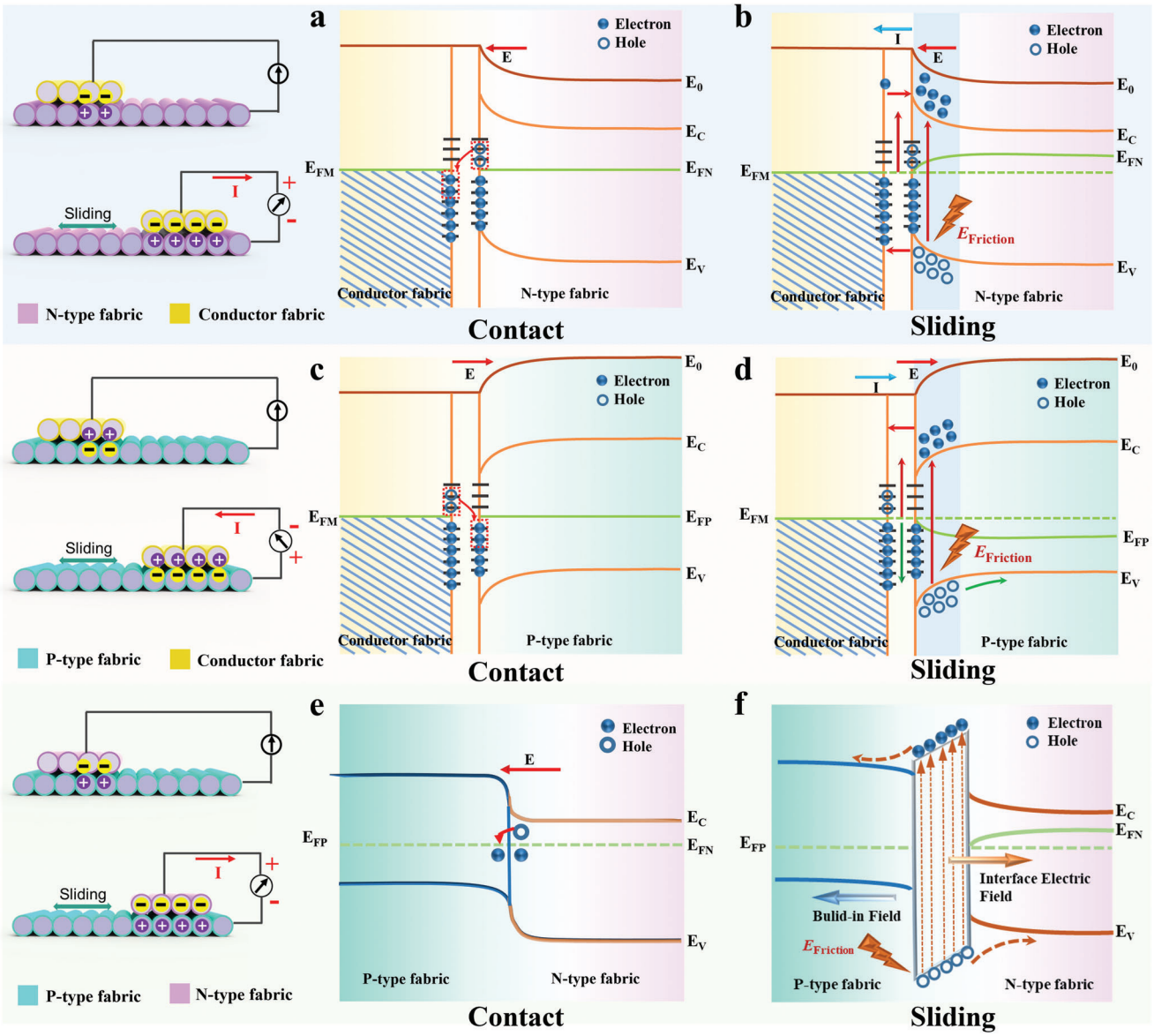

Figure 3. Schematic diagrams of the working principle and corresponding energy band structure of the AFDC-TENGs. a,b) The schematic diagram of charge transfer N/Ni–F under a) contact state and b) sliding state, respectively. c,d) The schematic diagrams illustrate the charge transfer process P/Ni–F in contact c) and sliding d) states, respectively. e,f) The schematic diagram of charge transfer N/P under e) contact state and f) sliding state, respectively (E_C is the bottom of the conductive band, E_{FM} is the Fermi level of the Ni-coated conductive fabric, E_{FN} the Fermi level of the n-type fabric, E_{FP} the Fermi level of the p-type fabric, E_V is the top of valence band, E_0 is the vacuum energy level).

fabrics. (Figure S14, Supporting Information). Furthermore, the wide selection of substrates materials also indicates the excellent adaptability of our p-type AFDC-TENG. As a wearable energy harvester, sliding distance is a crucial factor influencing the electrical output. when the p-type AFDC-TENG slides at a constant frequency. As shown in Figure 4b, the current increases with the increased sliding distance, which may be attributed to the increased charge collection area. In order to investigate the impact of area on electrical output, a systematic study of the length (L) and width (W) of the top triboelectric layer (Ni-coated conductive fabric) is conducted. When a constant force is applied to the p-type AFDC-TENG, the electrical output increases with the increase of the contact area between the bottom (p-type fabric) and top triboelectric layers (Figure 4c; Figure S15, Supporting Information). Moreover, it is observed that the current is stable at 0.29 μA with the change of length and width, when the area of the top triboelectric layer is kept (Figure 4d). This suggests that the length and width do not impact the collection of surface charge when the area remains the same. Similar conclusions are supported by the voltage variation (Figure S16, Supporting Information).

Furthermore, the electrical output of the p-type AFDC-TENG increases with the increase of the applied force. The effective contact area between the p-type fabric and the Ni-coated conductive fabric is increased under heavier objects, resulting in more

© 2023 Wiley-VCH GmbH

16146840, 0, Downloaded from https://onlinelibrary.wiley.com/doi/10.1002/aenm.202301178 by Georgia Institute Of Technology, Wiley Online Library on [15/06/2023]. See the Terms and Conditions (https://onlinelibrary.wiley.com/terms-and-conditions) on Wiley Online Library for rules of use; OA articles are governed by the applicable Creative Commons License

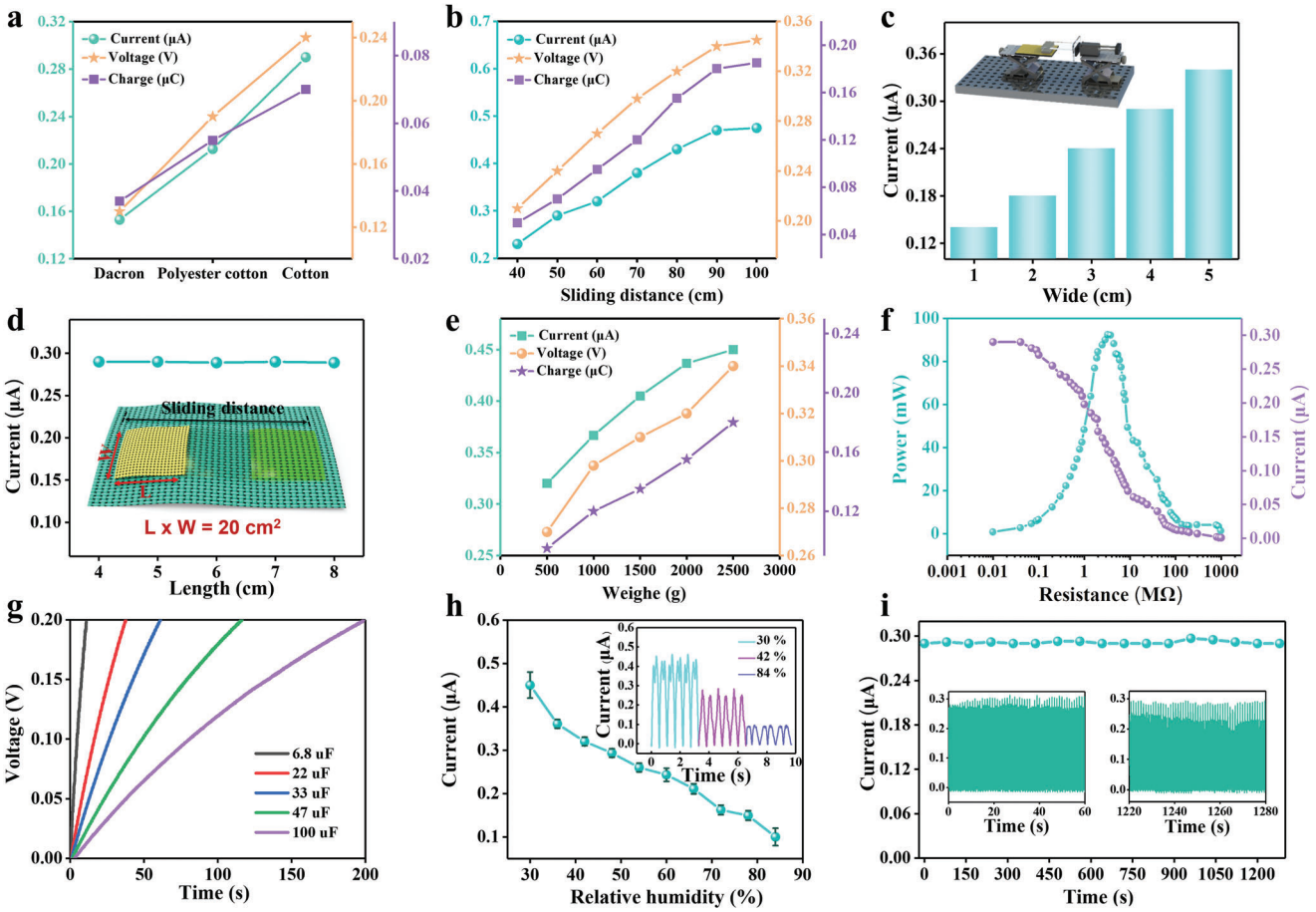

Figure 4. Electrical output of p-type AFDC-TENG with different factors. a,b) The current output of the p-type AFDC-TENG for a) different types of fabrics b) various sliding distances. c,d) Some structural parameters are studied on the output of the current, including the width (*W*), length (*L*), and constant area of the Ni-coated conductive fabric c) different widths d) constant area. e) Current of p-type AFDC-TENG at different pressures when the sliding distance is 5 cm. f) Variation of current and power density of p-type AFDC-TENG with different external load resistance. g) Charging curves of different capacitance capacities. h) Current of p-type AFDC-TENG for different *RH* values. The current values at *RH* levels of 18.9%, 58%, and 70.6% are displayed in the upper right corner. i) Stability test of the p-type AFDC-TENG under continuous impact for 1280 s. Detailed current of the early 60 s and the last 60 s at the insets exhibit.

tribo-charges on the surface, thereby increasing the electrical output. However, the effective contact area and electrical output reach saturation when the weight is large enough. Therefore, when the weight is ≈2.5 kg, the electrical output reaches saturation of ≈0.45 μA (Figure 4e). The output power densities are measured by connecting different external loads ranging from 10 kΩ to 1 GΩ (Figure 4f). Power density is a crucial parameter for energy harvesters. In order to discuss the average power change of p-type AFDC-TENG under different loads, the average power is calculated using the following formula:

$$P_{ave} = \frac{1}{T}\int_{o}^{T} I^2(t)\,Rdt \tag{5}$$

where $I(t)$ is the current across the resistor R at time t, and T is the integration time. When the load resistance was <10 MΩ, the output current almost remained constant. However, as the load resistance increased, the output current decreased. The maximum output power density of 45.5 mW m^{-2} has been achieved at a load resistance of 3.3 MΩ, indicating that our AFDC-TENG has great potential as a DC wearable power source. The capacitance also affects the voltage output. We tested voltage curves of different capacitors (6.8, 22, 33, and 100 μF) charged by p-type AFDC-TENG (Figure 4g). As the capacitance increases, the charging voltage decreases with a decrease charging rate. A 6.8 μF capacitor can charge up to 0.2 V within 10 s (measured with a frequency of 1 Hz, a sliding distance of 5 cm, and various types of resistors *R*). This study examines the impact of relative humidity (*RH*) on the output of AFDC-TENG. It is found that the *RH* can significantly affect the electrical output of AFDC-TENG, as illustrated in Figure 4h. Specifically, when the friction frequency is 1 Hz, the output current decreases as RH increases. With the increase of relative humidity, water layers appear on the surface of friction material, exacerbating the dissipation of surface charges in the friction layer. Moreover, the increase of surface Schottky barriers will also reduce the possibility of electron transfer. The long-term stability of the p-type AFDC-TENG is evaluated by performing continuous friction for 1280 s (Figure 4i). During the

© 2023 Wiley-VCH GmbH

16146840, 0, Downloaded from https://onlinelibrary.wiley.com/doi/10.1002/aenm.202301178 by Georgia Institute Of Technology, Wiley Online Library on [15/06/2023]. See the Terms and Conditions (https://onlinelibrary.wiley.com/terms-and-conditions) on Wiley Online Library for rules of use; OA articles are governed by the applicable Creative Commons License

entire test process, the generated current stabilized at 0.29 μA. Although the average output is decreased, the maximum signal remains at the same level. The illustrations provide a detailed representation of the current output during the initial and final 60 s intervals. The resistance and mass changes before and after long-term friction were tested (Figure S17, Supporting Information). When Ni-coated conductive fabric rubs against p-type fabric, with the increase in friction times, SWCNTs were deposited on cotton fabrics with a mass reduction of only 0.8 mg, indicating that SWCNTs adhere well to cotton fabric. In addition, the resistance of p-type fabrics is gradually decreasing. Due to the friction between p-type fabric and Ni-coated conductive fabric, which causes the surface of p-type fabric to be worn. In addition, after 40 min of friction, the current of p-type AFDC-TENG slightly decreased, which proves the high stability of AFDC-TENG. For wearable energy harvesting devices, AFDC-TENG can be well integrated into our clothing due to its excellent flexibility (Figure S18, Supporting Information). Current, voltage, and charge of AFDC-TENG integrated on the clothes show a downward trend, which the decrease of the effective contact area of the two materials during contact. These results demonstrate that the AFDC-TENG exhibits exceptional stability and durability. All these conclusions show that AFDC-TENG as a DC power supply can meet some needs in our daily life.

3. Conclusion

In summary, two functional fabrics, including p-type fabrics and n-type fabrics, were designed through simple chemical doping methods. Through the reciprocating friction between these two pairs of semiconductor fabrics and Ni-coated conductive fabrics, three kinds of AFDC-TENGs based on the tribovolatic effect are developed, which include P/Ni–F, N/Ni–F, and P/N. When Ni-coated conductive fabrics rub against p- and n-type fabrics, respectively, two opposite Schottky junctions are formed, resulting in DC outputs with opposite current directions. The potential DC output mechanisms of different types of AFDC-TENGs are elucidated through energy band diagrams. Specifically, the mutual frictions between different functional fabrics stimulate the excitation of electron–hole pairs at the interface, resulting in the DC generation in the external circuit, which demonstrates that the tribovoltaic effect can be effectively realized on textile materials. The influence of various parameters including contact area, sliding velocity, and applied pressure on the electrical output performance of AFDC-TENGs is analyzed in detail. It can be found that the number of carriers will increase with the increase of the effective contact area, sliding speed, and applied pressure, further increasing the output voltage and current. In addition, all the AFDC-TENGs exhibit excellent flexibility, breathability, and durability, which are fit for wearable usage. This study presents the first conceptual all-fabric DC power source, demonstrating its significant potential for the future application of wearable electronic products.

4. Experimental Section

Chemicals and Materials: The pristine SWCNT powder with a carbon purity of ≥85% was obtained from Shenzhen Nanotech port Co., Ltd. The average diameter of the SWCNTs was between 1 and 3 nm. Sodium dodecylbenzene sulfonate (SDBS) and cetyltrimethylammonium bromide (CTAB) were provided by Shanghai Aladdin Bio-Chem Technology Co., Ltd. Electroplated nickel conductive cloth from Shandong Yinlong New Material Technology Co., Ltd.

Preparation of p- and n-Type SWCNTs: The p- and n-type SWCNT solution inks were fabricated by an easy water–solution mixing procedure, with the addition of surfactant and SWCNTs in deionized water. At first, 100 mg SWCNT powder was mixed in 100 ml ultrapure water to prepare SWCNT suspension. Then, 100 mg SDBS or CTAB powder was added to the SWCNT suspension. The mixture was initially stirred for 5 min, then tip-sonicated for 60 min, sonicated for another 240 min, stirred for 30 min, and finally sonicate for 6 h.

Preparation of p- and n-Type Fabric: The resulting p- and n-type SWCNT inks were first centrifuged at the conditions of 5 min and 8000 rpm. The sediment at the bottom of the centrifugal tube was abandoned. The fabrics were then dip coated at the 60 s, and finally the p- and n-type SWCNT inks were dried in a vacuum oven at 60 °C for 20 min.

Characterization Techniques: The AFDC-TENG was driven using a linear motor (LinMot E1200) for electrical measurements, and the I_{SC}, V_{OC}, and Q_{SC} were measured using an electrometer (Keithley, model 6514). If no special declaration, the area of the upper Nickel electrode was set to be 4×5 cm^2. The Raman spectra was recorded with a laser confocal Raman spectrometer (LabRAM HR Evolution) equipped with a 532 nm laser, and a grating of 1800 gr mm^{-1}. All Raman spectra were collected in the range of 90–3500 cm^{-1} with acquisition times of 30 s. The surface topography of p- and n-type SWCNT were characterized with scanning electron microscopy (Nova NanoSEM 450) under the acceleration voltage of 5 KV and the acceleration of 10 μA. Energy dispersive X-ray spectroscopic (EDX) mapping was conducted using a Thermo Fisher Themsis-Z S/TEM equipped with a Super-X EDS detector system. Ultraviolet absorption spectroscopy (UPS) was used to measure the work function (Thermo ESCALAB 250XL).

Supporting Information

Supporting Information is available from the Wiley Online Library or from the author.

Acknowledgements

The authors are grateful for the support received from the National Natural Science Foundation of China (grant no. 22109012), the Natural Science Foundation of the Beijing Municipality (grant nos. L222037 and 2212052), the National Key R & D Project from the Ministry of Science and Technology (grant no. 2021YFA1201601), and the Fundamental Research Funds for the Central Universities (grant no. E1E46805). No formal approval for the experiments involving human volunteers was required. The volunteers took part following informed consent.

Conflict of Interest

The authors declare no conflict of interest.

Author Contributions

K.D. conceived this idea. K.D. and Z.L.W. led this project. T.L. performed all of the experiments. R.C. and C.W. helped with the analysis of experimental results. E.S., T.J., F.S., and X.P. helped with the data analysis. All of the authors discussed the results and contributed to the manuscript preparation.

Data Availability Statement

The data that support the findings of this study are available from the corresponding author upon reasonable request.

© 2023 Wiley-VCH GmbH

16146840, 0, Downloaded from https://onlinelibrary.wiley.com/doi/10.1002/aenm.202301178 by Georgia Institute Of Technology, Wiley Online Library on [15/06/2023]. See the Terms and Conditions (https://onlinelibrary.wiley.com/terms-and-conditions) on Wiley Online Library for rules of use; OA articles are governed by the applicable Creative Commons License

Keywords

all fabrics, direct current, semiconductor doping, triboelectric nanogenerators, tribovoltaic effects

Received: April 20, 2023
Revised: May 22, 2023
Published online:

[1] a) C. Ning, G. Zheng, K. Dong, *Adv. Sens. Res.* **2023**, *2*, 2200044; b) T. He, H. Wang, J. Wang, X. Tian, F. Wen, Q. Shi, J. S. Ho, C. Lee, *Adv. Sci.* **2019**, *6*, 1901437; c) F. Sheng, B. Zhang, R. Cheng, C. Wei, S. Shen, C. Ning, J. Yang, Y. Wang, Z. Wang, K. Dong, *Nano Res. Energy* **2023**, http://doi.org/10.26599/NRE.2023.9120079.

[2] a) K. Dong, X. Peng, Z. L. Wang, *Adv. Mater.* **2020**, *32*, 1902549; b) L. Lin, V. G. N. Thyagaraja, R. Ranjith, R. Yang, S. Ciampi, J. Chen, J. Liu, *Nano Energy* **2023**, *107*, 108163; c) S. Lin, Z. L. Wang, *Mater. Today* **2022**, *62*, 111; d) T. He, Q. Shi, H. Wang, F. Wen, T. Chen, J. Ouyang, C. Lee, *Nano Energy* **2019**, *57*, 338.

[3] a) H. Li, J. Wen, Z. Ou, E. Su, F. Xing, Y. Yang, Y. Sun, Z. L. Wang, B. Chen, *Adv. Funct. Mater.* **2023**, *33*, 2212207; b) Y. Huang, D. Liu, X. Gao, J. Zhu, Y. Zhang, M. Zhang, *Adv. Funct. Mater.* **2022**, *33*, 2209484; c) C. Ning, K. Dong, R. Cheng, J. Yi, C. Ye, X. Peng, F. Sheng, Y. Jiang, Z. L. Wang, *Adv. Funct. Mater.* **2020**, *31*, 2006679; d) S. Lin, L. Xu, L. Zhu, X. Chen, Z. L. Wang, *Adv. Mater.* **2019**, *31*, 1901418; e) X. Xu, J. Li, X. Tao, Q. Yan, H. Wu, Z. Guan, L. Liu, X. Chen, W. Ou-Yang, *Nano Energy* **2022**, *94*, 106957; f) C. Ning, C. Wei, F. Sheng, R. Cheng, Y. Li, G. Zheng, K. Dong, Z. L. Wang, *Nano Res.* **2023**, *16*, 7518; g) J. Zhu, M. Cho, Y. Li, T. He, J. Ahn, J. Park, T.-L. Ren, C. Lee, I. Park, *Nano Energy* **2021**, *86*, 106035.

[4] R. Cheng, C. Ning, P. Chen, F. Sheng, C. Wei, Y. Zhang, X. Peng, K. Dong, Z. L. Wang, *Adv. Energy Mater.* **2022**, *12*, 2201532.

[5] C. Chen, H. Guo, L. Chen, Y. C. Wang, X. Pu, W. Yu, F. Wang, Z. Du, Z. L. Wang, *ACS Nano* **2020**, *14*, 4585.

[6] Y. Du, S. Fu, C. Shan, H. Wu, W. He, J. Wang, H. Guo, G. Li, Z. Wang, C. Hu, *Adv. Funct. Mater.* **2022**, *32*, 2208783.

[7] S. Lin, X. Chen, Z. L. Wang, *Nano Energy* **2020**, *76*, 105070.

[8] J. Luo, L. Xu, W. Tang, T. Jiang, F. R. Fan, Y. Pang, L. Chen, Y. Zhang, Z. L. Wang, *Adv. Energy Mater.* **2018**, *8*, 1800889.

[9] a) R. Cheng, K. Dong, P. Chen, C. Ning, X. Peng, Y. Zhang, D. Liu, Z. L. Wang, *Energy Environ. Sci.* **2021**, *14*, 2460; b) G. Liu, R. Luan, Y. Qi, L. Gong, J. Cao, Z. Wang, F. Liu, J. Zeng, X. Huang, Y. Qin, S. Dong, Y. Feng, L.-B. Huang, C. Zhang, *Nano Energy* **2023**, *106*, 108075.

[10] a) S. Dong, T. Bu, Z. Wang, Y. Feng, G. Liu, J. Zeng, Z. Wang, J. Cao, Z. Zhang, F. Liu, C. Zhang, *Adv. Energy Mater.* **2023**,*13*, 2300079; b) L. Ren, A. Yu, W. Wang, D. Guo, M. Jia, P. Guo, Y. Zhang, Z. L. Wang, J. Zhai, *Nano Lett.* **2021**, *21*, 10099; c) M. Zheng, S. Lin, L. Zhu, Z. Tang, Z. L. Wang, *Adv. Mater. Interfaces* **2021**, *9*, 2101757.

[11] a) S. Sriphan, N. Vittayakorn, *Mater. Today Nano* **2023**, *22*, 100318; b) C. Xu, J. Yu, Z. Huo, Y. Wang, Q. Sun, Z. L. Wang, *Energy Environ. Sci.* **2023**, *16*, 983.

[12] a) X. Luo, L. Liu, Y. C. Wang, J. Li, A. Berbille, L. Zhu, Z. L. Wang, *Adv. Funct. Mater.* **2022**, *32*, 2113149; b) Z. Zhang, D. Jiang, J. Zhao, G. Liu, T. Bu, C. Zhang, Z. L. Wang, *Adv. Energy Mater.* **2020**, *10*, 1903713; c) M. Zheng, S. Lin, Z. Tang, Y. Feng, Z. L. Wang, *Nano Energy* **2021**, *83*, 105810.

[13] a) C.-W. Chu, C.-F. Sung, Y.-Z. Lee, K. Cheng, *Org. Electron.* **2008**, *9*, 262; b) Q. Luo, K. Xiao, J. Zhang, W. Sun, *ACS Appl. Electron. Mater.* **2022**, *4*, 4212; c) D. Yang, L. Zhang, N. Luo, Y. Liu, W. Sun, J. Peng, M. Feng, Y. Feng, H. Wang, D. Wang, *Nano Energy* **2022**, *99*, 107370.

[14] a) K. Dong, X. Peng, J. An, A. C. Wang, J. Luo, B. Sun, J. Wang, Z. L. Wang, *Nat. Commun.* **2020**, *11*, 2868; b) R. Yang, Z. He, S. Lin, W. Dou, Z. L. Wang, H. Wang, J. Liu, *Nano Lett.* **2022**, *22*, 9084; c) B. Yoon, S. J. Choi, T. M. Swager, G. F. Walsh, *ACS Sens.* **2021**, *6*, 3056; d) M. Zheng, S. Lin, L. Xu, L. Zhu, Z. L. Wang, *Adv. Mater.* **2020**, *32*, 2000928.

[15] J. Meng, Z. H. Guo, C. Pan, L. Wang, C. Chang, L. Li, X. Pu, Z. L. Wang, *ACS Energy Lett.* **2021**, *6*, 2442.

[16] Y.-S. Lee, S. Jeon, D. Kim, D.-M. Lee, D. Kim, S.-W. Kim, *Nano Energy* **2023**, *106*, 108066.

[17] S. Wang, J. Wu, F. Yang, H. Xin, L. Wang, C. Gao, *ACS Appl. Mater. Interfaces* **2021**, *13*, 26482.

[18] C. K. Mytafides, L. Tzounis, G. Karalis, P. Formanek, A. S. Paipetis, *ACS Appl. Mater. Interfaces* **2021**, *13*, 11151.

[19] X. Cheng, X. Wang, G. Chen, *J. Mater. Chem. A* **2018**, *6*, 19030.

[20] a) N. Ishiyama, T. Yoshioka, T. Kaji, M. Hiramoto, *Appl. Phys. Express* **2013**, *6*, 012301; b) J. Meng, C. Pan, L. Li, Z. H. Guo, F. Xu, L. Jia, Z. L. Wang, X. Pu, *Energy Environ. Sci.* **2022**, *15*, 5159; c) R. Yang, R. Xu, W. Dou, M. Benner, Q. Zhang, J. Liu, *Nano Energy* **2021**, *83*, 105849; d) F. Wen, Z. Sun, T. He, Q. Shi, M. Zhu, Z. Zhang, L. Li, T. Zhang, C. Lee, *Adv. Sci.* **2020**, *7*, 2000261.

[21] P. G. Collins, K. Bradley, M. Ishigami, A. Zettl, *Science* **2000**, *287*, 1801.

[22] Z. Zhang, Z. Wang, Y. Chen, Y. Feng, S. Dong, H. Zhou, Z. L. Wang, C. Zhang, *Adv. Mater.* **2022**, *34*, 2200146.

[23] Z. L. Wang, A. C. Wang, *Mater. Today* **2019**, *30*, 34.

© 2023 Wiley-VCH GmbH

16146840, 0, Downloaded from https://onlinelibrary.wiley.com/doi/10.1002/aenm.202301178 by Georgia Institute Of Technology, Wiley Online Library on [15/06/2023]. See the Terms and Conditions (https://onlinelibrary.wiley.com/terms-and-conditions) on Wiley Online Library for rules of use; OA articles are governed by the applicable Creative Commons License